SEXTEN CENTER
FOR ASTROPHYSICS
RICCARDO GIACCONI

Cosmic GRB formation rate studied on the largest homogeneous sample of bursts detected over a broad energy band

Anastasia Tsvetkova
University of Cagliari

HIGH REDSHIFT GAMMA-RAY-BURSTS IN THE JWST ERA
Sexten, Italy
09-13 January 2023

Motivation

- ~450 GRBs with reliable *z* by 2023;
- The unbiased comparison between GRBs;
- Collapsar model implies that the GRB formation rate should in principle trace the cosmic star formation rate (SFR)
- Possibility to test GRB progenitor and emission models;

Luminosity and energy release functions

Without loss of generality, the total luminosity function (LF; number of bursts per unit luminosity) $\Phi(L_{iso}, z)$ can be rewritten as

$$\Phi(L_{\rm iso}, z) \;=\; \rho(z)\phi(L_{\rm iso}/g(z), \alpha_s)/g(z)$$

Lloyd-Ronning (2002)

$\rho(z)$ – GRB formation rate (GRBFR)

$\phi(L_{\rm iso}/g(z))$ – local LF

$g(z) = (1+z)^{\delta}$ – luminosity evolution (Lloyd-Ronning 2002)

α_s – shape of the LF (Yonetoku 2004)

Examples of evolving astrophysical objects:

- Galaxies: the local luminosity function varies for early- and late-type galaxies (Marzke et al. 1994)
- Quasars: L ~ $(1+z)^3$, z<1.5 (Boyle 1993; Hewett, Foltz, & Chaffee 1993); L ~ $(1+z)^{1.5}$, z < 3 (Hewett et al. 1993)

Luminosity (energy release) evolution

$$\tau = \frac{\sum_i (R_i - E_i)}{\sqrt{\sum_i V_i}}$$

$$E_i = (N_i + 1)/2$$

$$V_i = (N_i^2 - 1)/12$$

Luminosity evolution

$$g(z) = (1+z)^\delta$$

Local (non-evolving) luminosity

$$L' = L/g(z)$$

Local LF (in the comoving frame)

$$\psi(L')(1+z)^{\delta_{\mathrm{L}}}$$

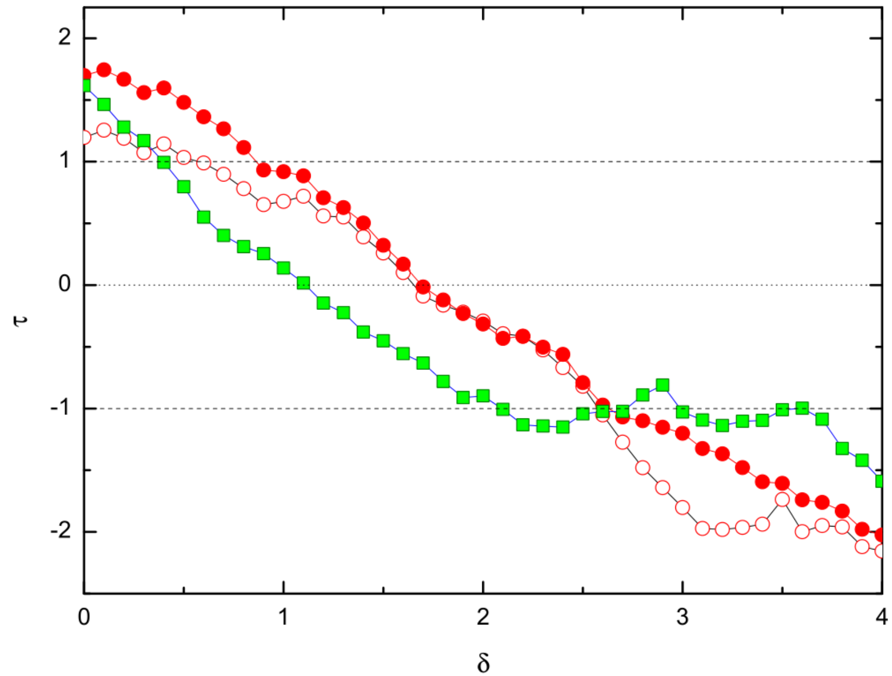

Red filled circles : per-burst truncation flux $F_{lim,i}$;

red open circles: monolithic F_{lim} = 2×10^{-6} erg cm^{-2} s^{-1} ;

green squares: S_{lim} = 4.3×10^{-6} erg cm^{-2} .

L_{iso}: τ_0 = 1.7 $\quad \delta_L = 1.7^{+0.9}_{-0.9}$ $(1\sigma\ \mathrm{CL})$

E_{iso}: τ_0 = 1.6 $\quad \delta_E = 1.1^{+1.5}_{-0.7}$

⇨ GRBs were brighter in the past

Non-parametric statistical techniques for a truncated data sample

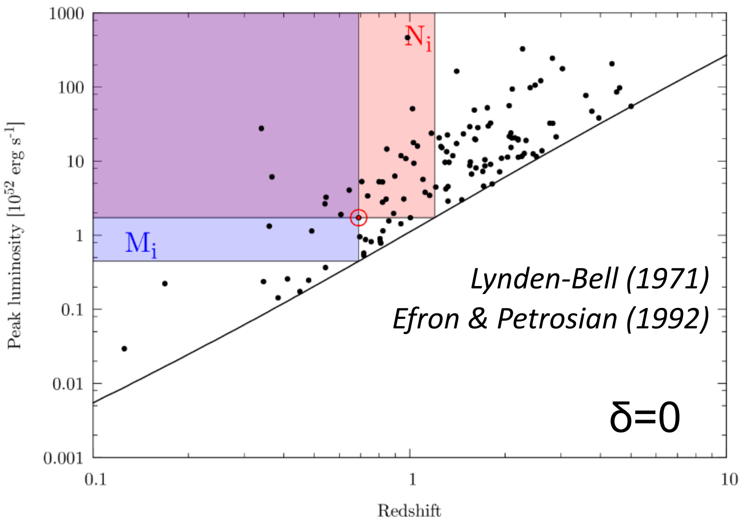

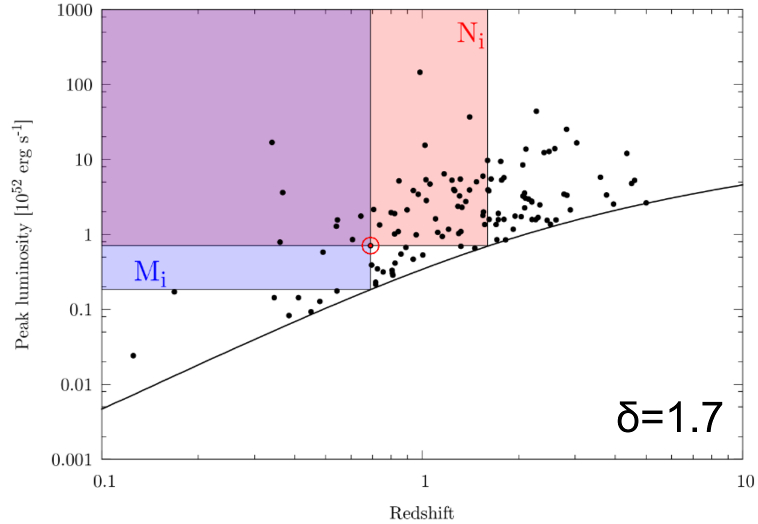

Associated sets:

M$_i$: $J'_i = \{j | z_j < z_i, L_j > L_{\rm lim,i}, L_{\rm i} > L_{\rm lim,j}\}$

$$L_j > L_i^{\rm lim} \Leftrightarrow z_j^{\rm lim} > z_i$$

N$_i$: $J_i = \{j | L_j > L_i, L_i > L_{\rm lim,j}\}$

$$\Updownarrow$$

$$J_i = \{j | L_j > L_i, z_j < z_{\rm lim,i}\}$$

Cumulative GRB number

$$\ln \psi(z_i) = \sum_{j=2}^{i} \ln\left(1 + \frac{1}{M_j}\right)$$

Cumulative LF

$$\ln \psi(L'_i) = \sum_{j=2}^{i} \ln\left(1 + \frac{1}{N'_j}\right)$$

Luminosity (energy release) evolution

The evolution of the amount of energy (per unit time) emitted by the GRB progenitor (Lloyd-Ronning 2002)

The jet opening angle evolution (the jet evolution) is rejected:

ρ = -0.4
P = 0.01
N = 43

The evolution of the GRB progenitor (massive star) itself: The stellar initial mass function (IMF) was “top-heavy” at high redshift (Larson 1998 and references therein, Malhotra & Rhoads 2002)

Progenitors lost less mass before collapse

The stellar metallicities were lower

The mass scale of the IMF was higher in the earlier stages of the Universe

Temperature in star-forming clouds in the early universe was probably higher

- The cosmic background temperature was higher;
- The metallicity was lower, which implies lower cooling rates and therefore higher temperatures on average;
- The heating rates were probably higher in the past because the SFR per unit volume was higher, leading to more intense radiation fields at high redshifts.

Main past, present, and future space-based missions for GRB science

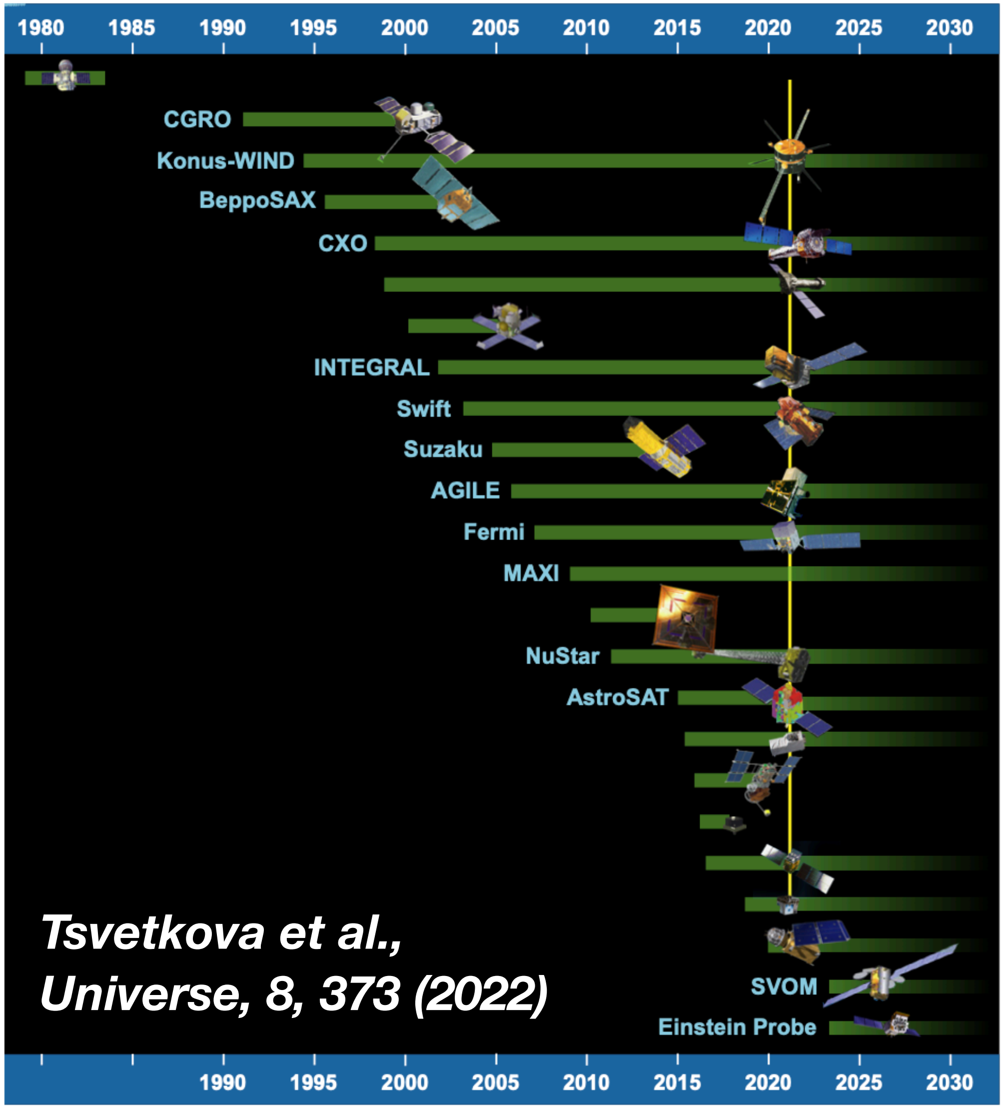

Swift/BAT, *Fermi*/GBM, Konus-*WIND*

Table 1. Comparison of Konus-Wind, Swift-BAT, and Fermi-GBM properties.

	KW	BAT	GBM
Crystal	NaI(Tl)	CdZnTe	NaI(Tl)/BGO
Number of detectors	2	– [a]	12/2
Diameter (cm)	12.7	–	12.7/12.7
Thickness(cm)	7.5	–	1.27/12.7
Approx. max. eff. area (cm^2)	160	5200	120/110
Energy range	20 keV–20 MeV [b]	14–150 keV [c]	8 keV–40 MeV
Approx. sensitivity (erg cm^{-2} s^{-1})	5×10^{-7}	1×10^{-8}	5×10^{-8}
FoV (sr)	4π	1.4 [d]	> 8
Operation time (yrs)	27	17	13
SGRB-to-LGRB rate	1:5	1:9	1:5

[a]: BAT is an assembly of 32,768 planar CdZnTe detectors (4×4 mm^2 large, 2 mm thick) to form a 1.2 m $\times$ 0.6 m sensitive area; [b]: Drifts with time; [c]: For coded FoV and up to 350 keV with no position information; [d]: For >50% coded FoV; ~2.2 sr for >10% coded FoV.

Tsvetkova et al., Universe, 8, 373 (2022)

Konus-*Wind* experiment

- The Konus-Wind (KW) is aimed primarily at GRB and SGR studies;
- Launched on November 1, 1994: 28 years of continuous operation;
- Now in orbit near L_1, up to 2.1 million km (~7 light s) from Earth;
- Observation statistics (triggers):
  2900 – GRBs (Fermi ~1500, BATSE ~2700, Swift ~1150), 260 – SGRs, 1000 – SFs.

Advantages

- Wide energy band;
- Exceptionally stable background;
- The orbit of s/c excepts interferences from radiation belts and the Earth occultation;
- Continuous observations of all sky;
- Duty circle 95%;
- Observes almost all bright events (>10^{-6} erg cm^{-2} s^{-1}).

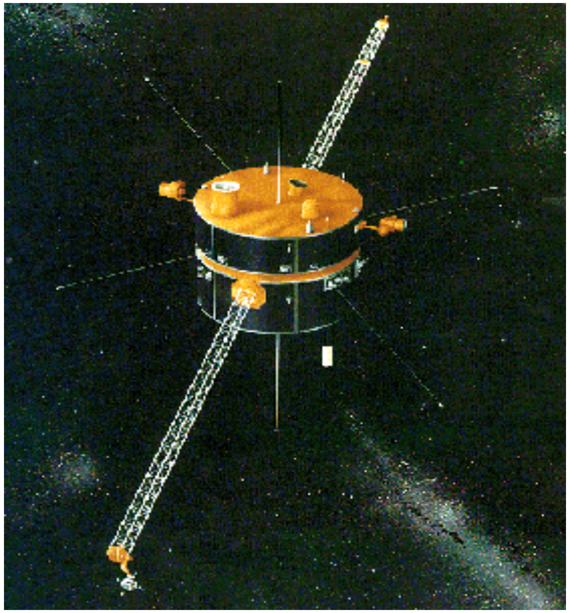

Konus-*Wind* experiment

- Two NaI detectors (S1 and S2) are located on opposite faces of spacecraft, observing correspondingly the southern and northern celestial hemispheres;
- ~100-160 cm^2 effective area;
- Light curves (LCs) in three energy windows:
  - G1 (~20–80 keV, at present);
  - G2 (~80–300 keV);
  - G3 (~300–1200 keV);
- Two modes:
- Waiting mode: G1, G2, G3 @ 2.944 s resolution;
- Triggered mode:
- LC res. is 2 ms –256 ms, from T_0-0.512 s to T_0+230 s;

  128-ch spectra (20 keV – 20 MeV).

The KW burst sample

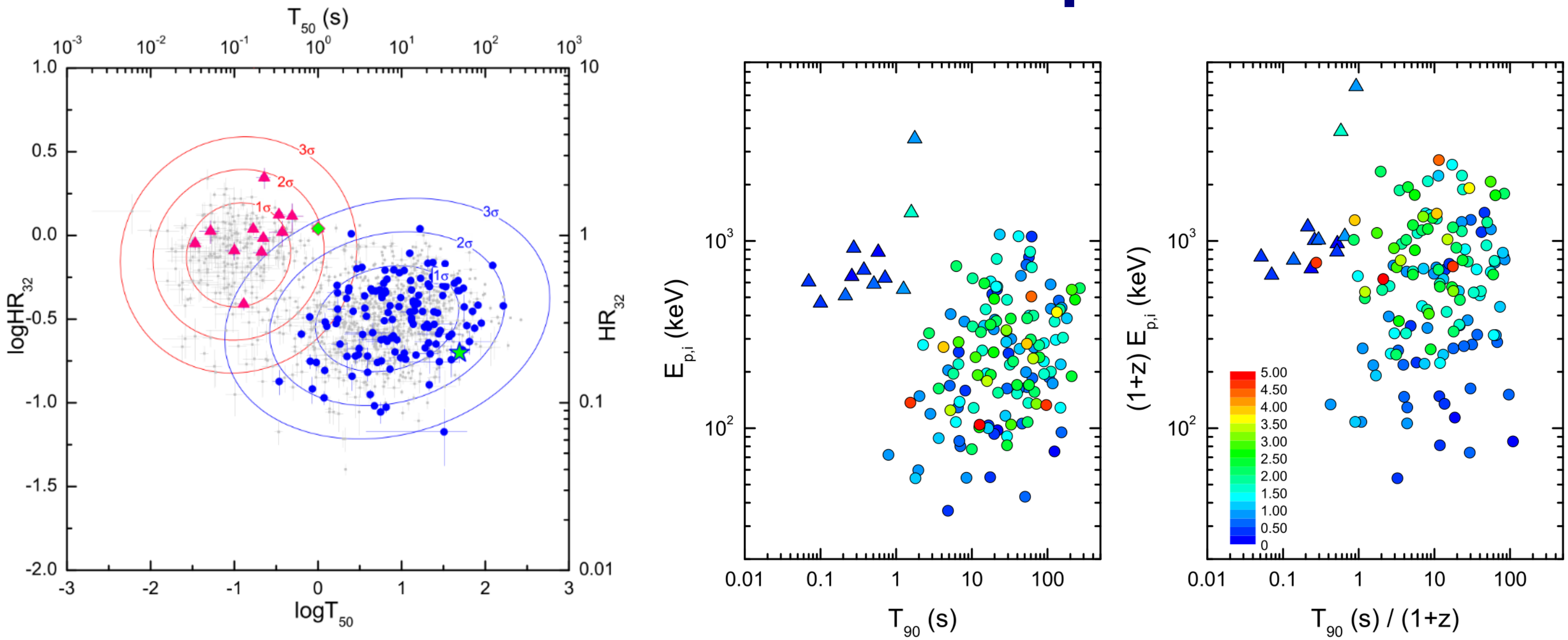

- 171 triggered GRBs (1997 Feb to 2018)
  14 Type I (the merger-origin, typically short/hard) GRBs
- 167 waiting-mode GRBs simultaneously detected by Swift/BAT
  4 short GRBs, 3 XRFs
- $0.04 \le z \le 9.4$
- 317 collapsar-origin GRBs

$3\cdot10^{49}$ erg < E_{iso} < $6\cdot10^{54}$ erg
$2\cdot10^{48}$ erg s^{-1} < L_{iso} < $5\cdot10^{54}$ erg s^{-1}

Hardness-duration distribution

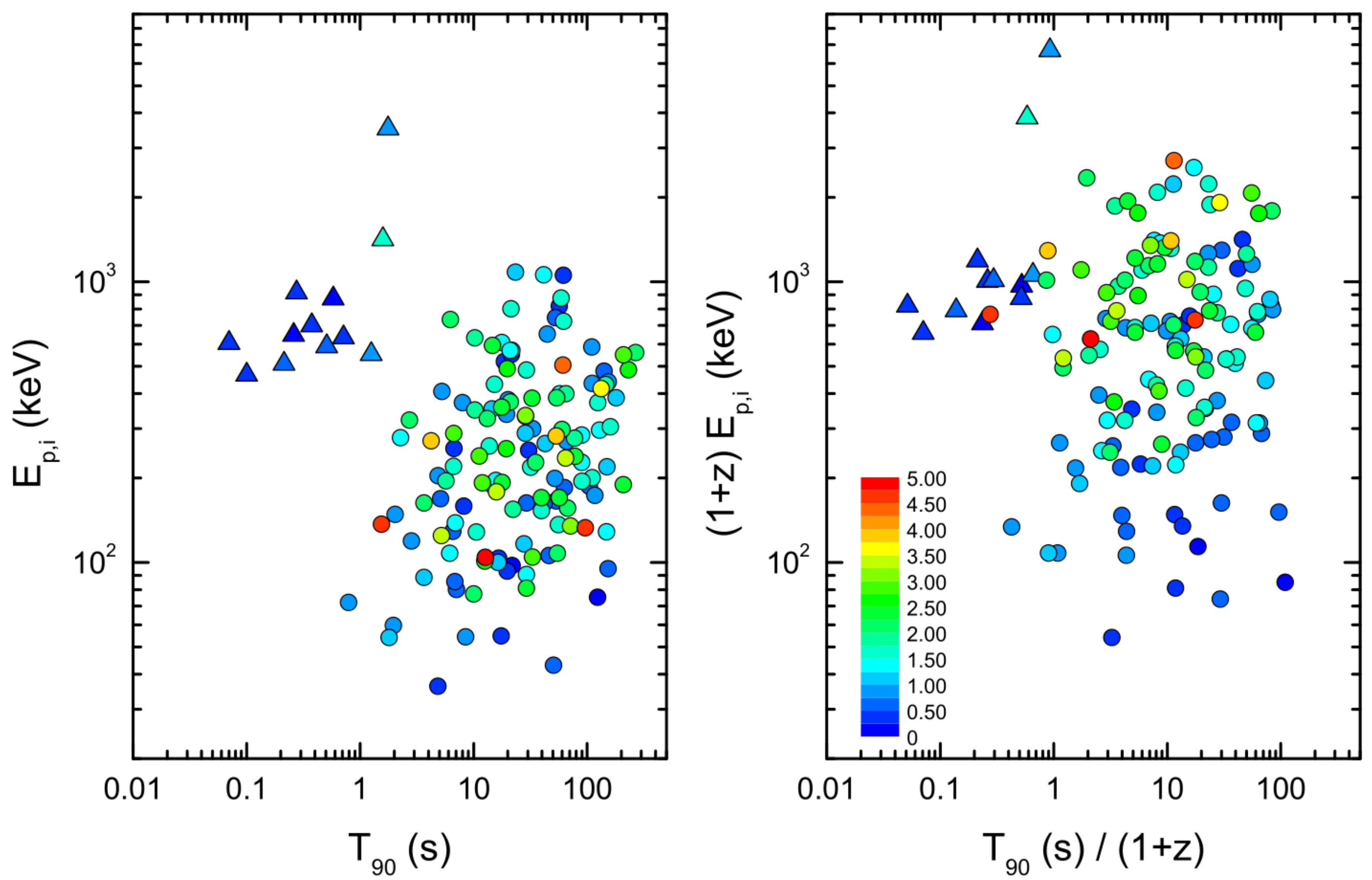

Hardness-duration distribution

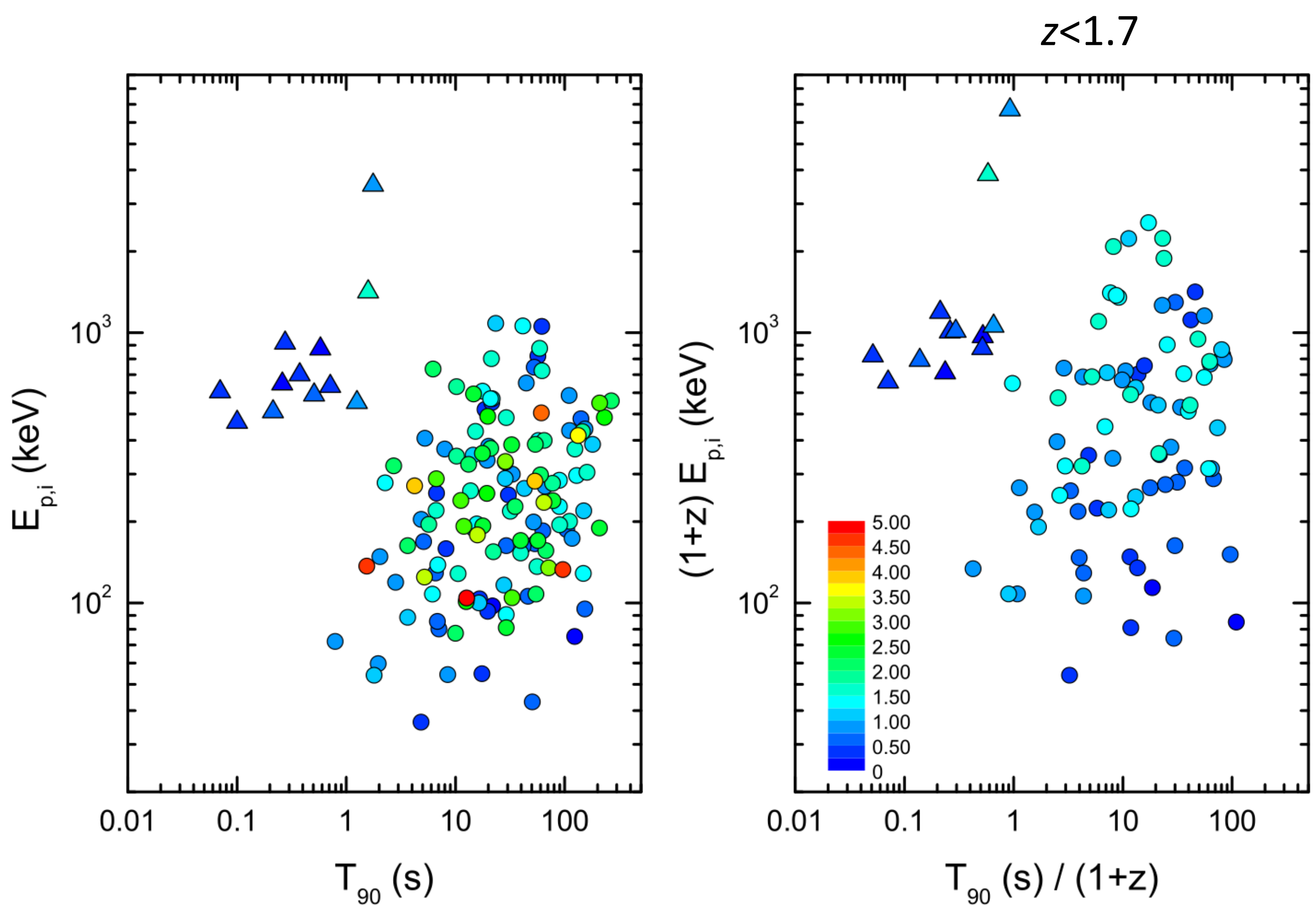

Hardness-duration distribution

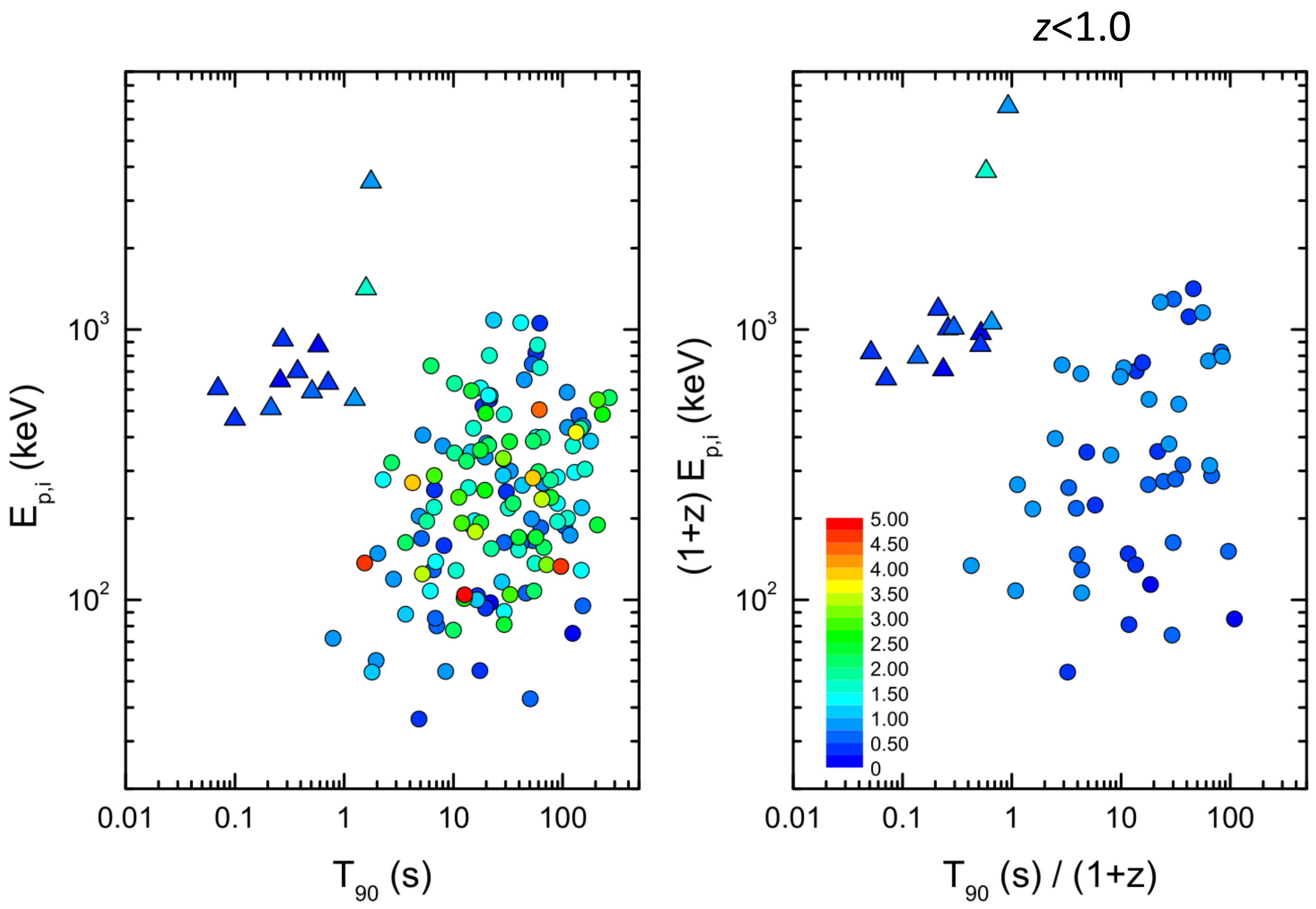

Selection effects

Dependence of the limiting KW energy flux on E_p

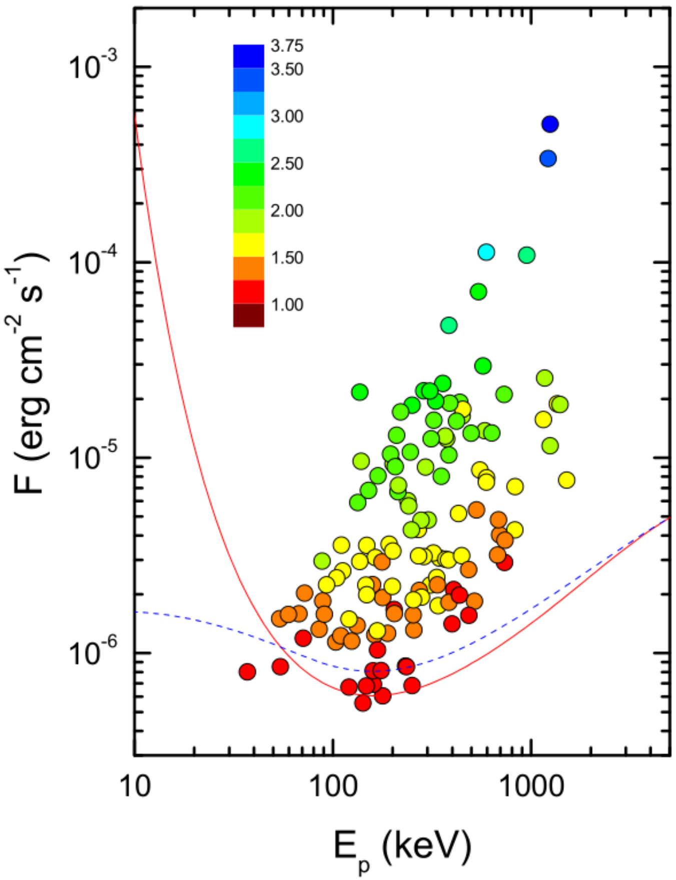

Trigger threshold: 9σ in G2: ~80 – 300 keV

Solid line: CPL (α= -1)

Dashed line: Band (α= -1, β = -2.5)

Incident angles: 60°

Band (2003)

Selection effects: triggered mode

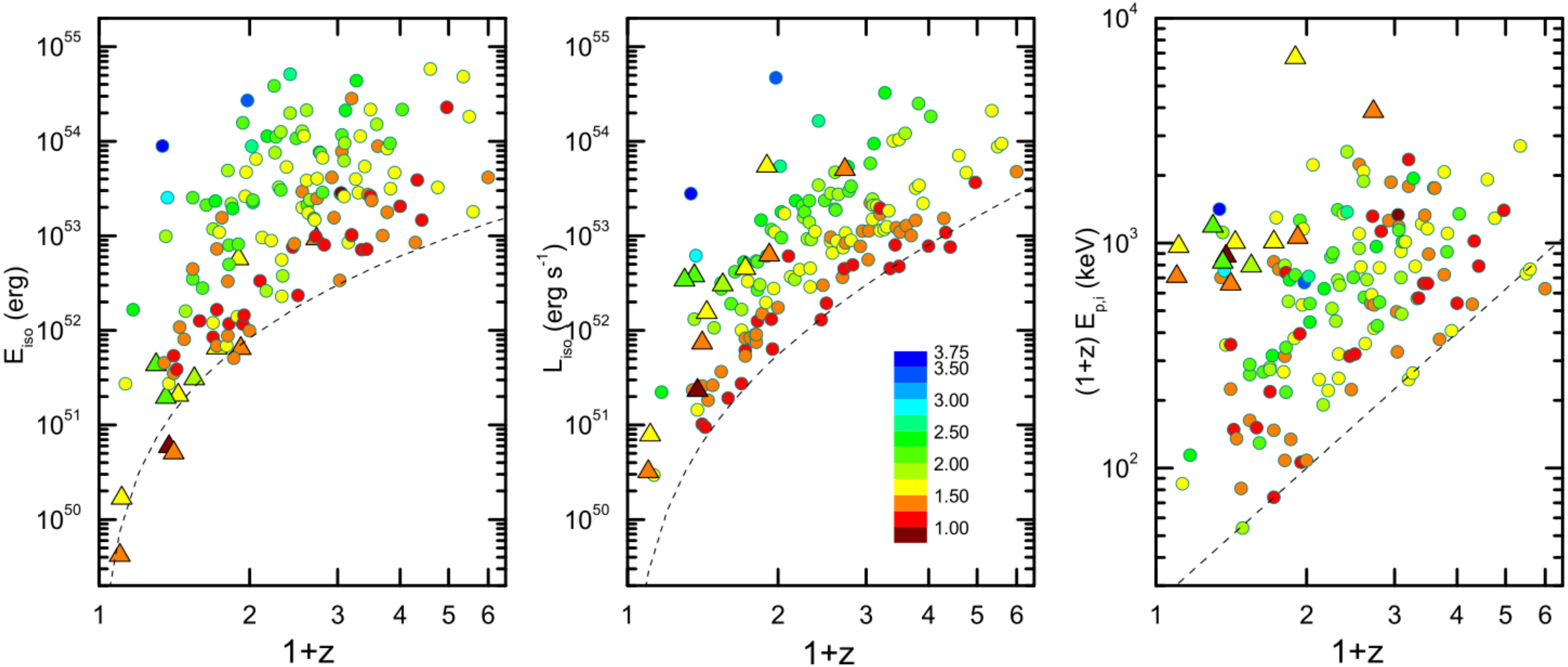

$S_{lim} \sim 3\times10^{-6}$ erg cm^{-2} $F_{lim} \sim 1\times10^{-6}$ erg cm^{-2} s^{-1} $E_{p,p,z} \sim 25(1+z)^2$ keV

Selection effects: waiting mode

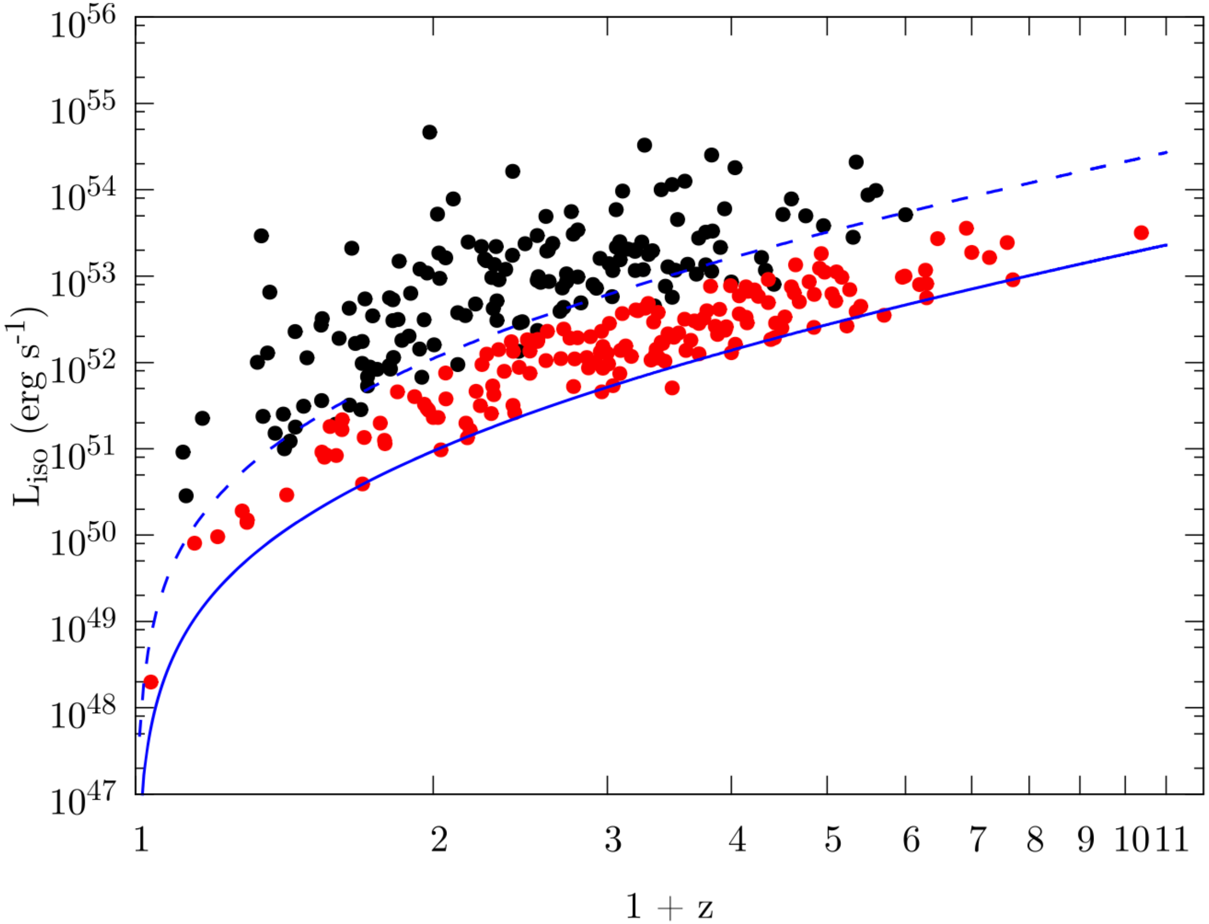

S_{lim} ~1.6×10^{-6} erg cm^{-2} ,
F_{lim} ~1.7×10^{-7} erg cm^{-2} s^{-1}

Black symbols show triggered bursts. Red symbols show the waiting-mode sample. The observer-frame flux limits F_{peak} are shown by a dashed line (triggered bursts) and a solid line (the full KW sample).

Selection effects and luminosity (energy release) evolution

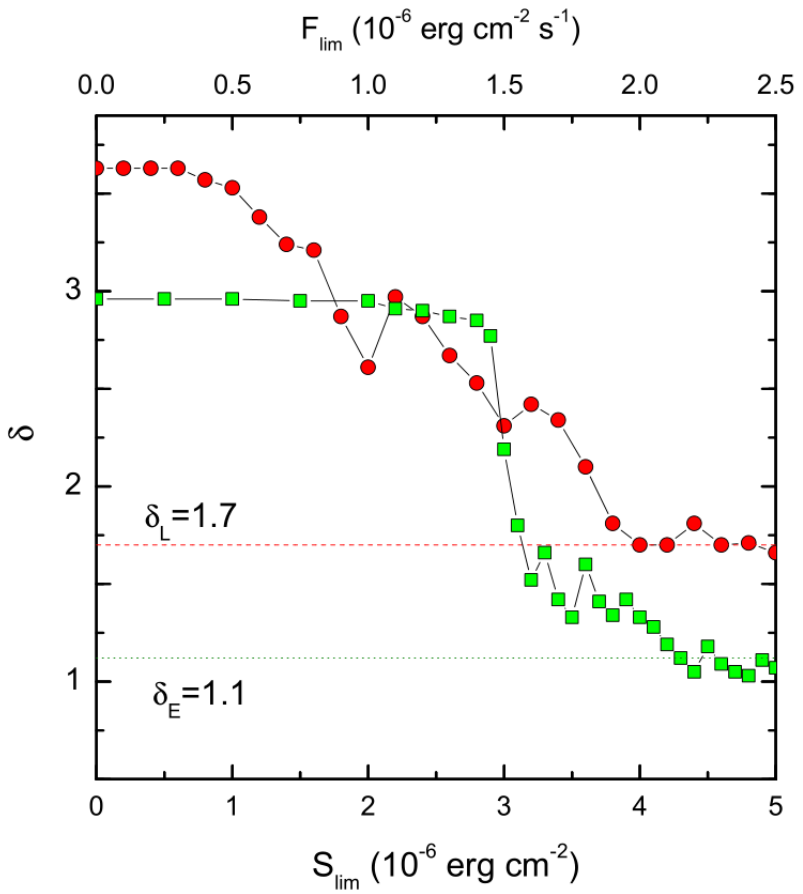

Red circles: Luminosity;
Green squares: Energy release.

$F_{lim} = 2\times10^{-6}$ erg cm^{-2} s^{-1} ;
$S_{lim} = 4.3 \times 10^{-6}$ erg cm^{-2} .

GRB formation rate: triggered mode

The low-*z* GRBFR excess over SFR is in agreement with the results reported in Yu et al. (2015) and Petrosian et al. (2015).

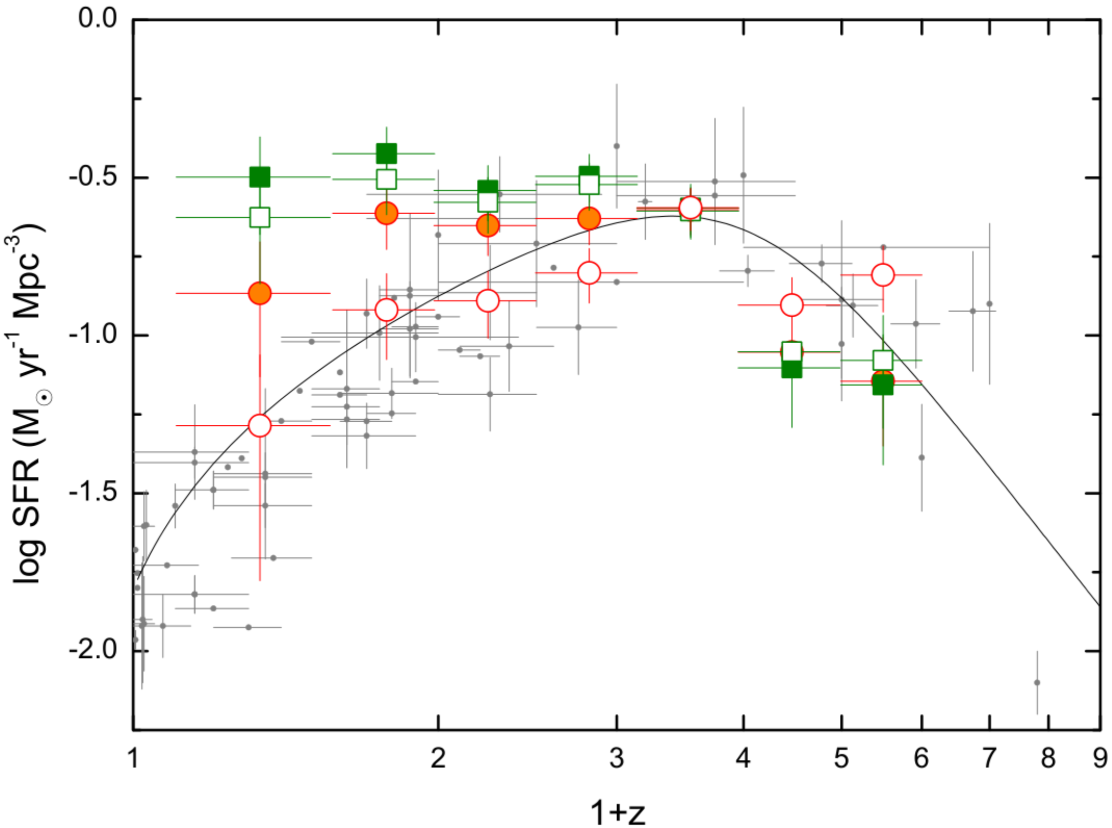

Cumulative rate evolution:

$$\ln \psi(z_i) = \sum_{j=2}^{i} \ln\left(1 + \frac{1}{M_j}\right)$$

Comoving density rate:

$$\rho(z) = \frac{d\psi}{dz}(1+z)\left(\frac{dV(z)}{dz}\right)^{-1}$$

Differential comoving volume:

$$\frac{dV(z)}{dz} = \frac{4\pi D_{\rm H} D_{\rm M}^2}{E(z)}$$

D_M is the transverse comoving distance

Hubble distance: $D_{\rm H} = c/H_0$

Normalized Hubble parameter:

$$E(z) = \sqrt{\Omega_{\rm M}(1+z)^3 + \Omega_\Lambda}$$

SFR: Hopkins (2004), Bouwens et al. (2011), Hanish et al. (2006), Thompson et al. (2006), Li (2008).

L_{iso}: red open circles: no luminosity evolution; red filled circles: δ_L= 1.7;

E_{iso}: green open squares: no energy evolution; green filled squares: δ_E = 1.1.

GRB formation rate: waiting mode

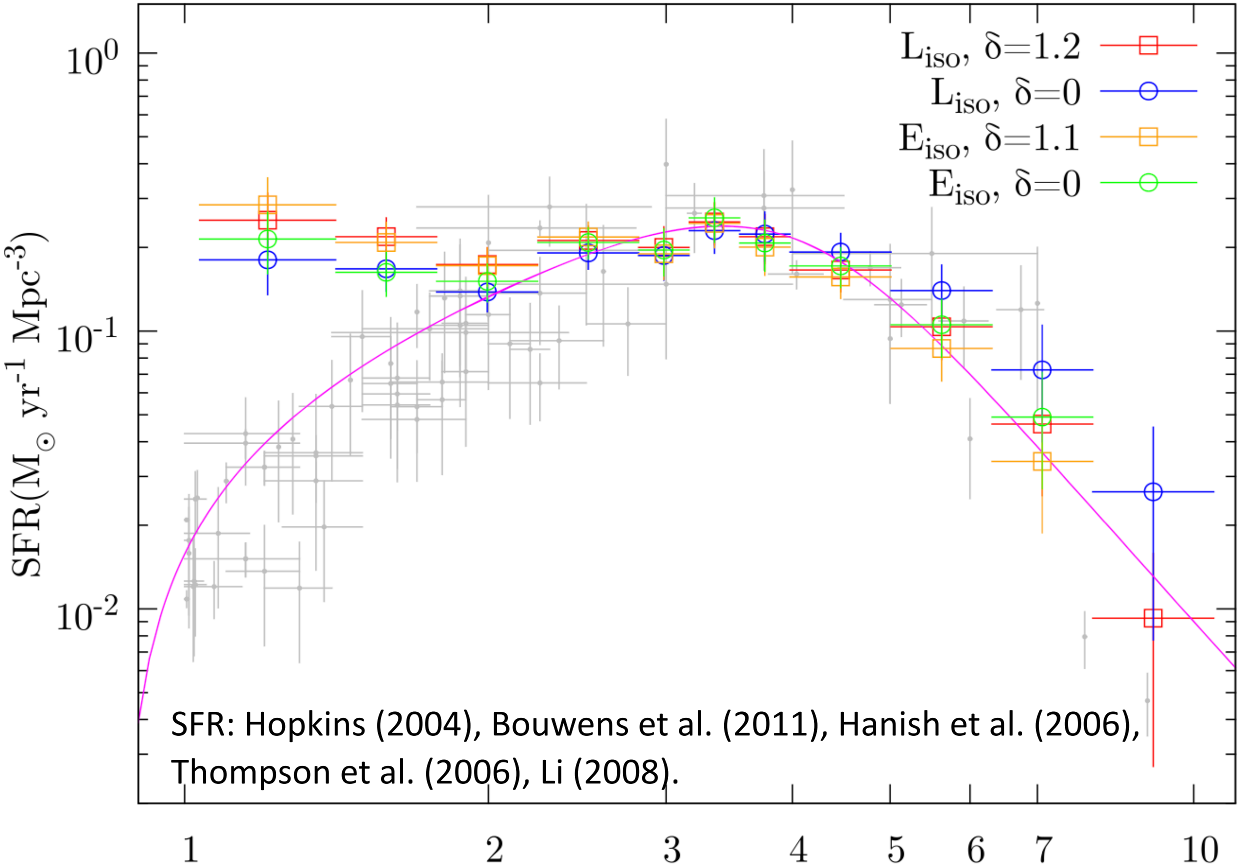

Preference of long GRBs for low-mass galaxies and low-metallicity environments, which are not unbiased tracers of the star-formation rate at low redshifts (Lloyd-Ronning et al. 2019).

Presence of selection effects based on the incompleteness of the sample: it is easier to measure the redshifts of nearest GRBs thereby creating a bias toward them, which, in turn, will lead to the relative excess of low-z bursts over the rest of the unbiased sample (Pescalli et al. 2016)

GRB formation rate: modeling

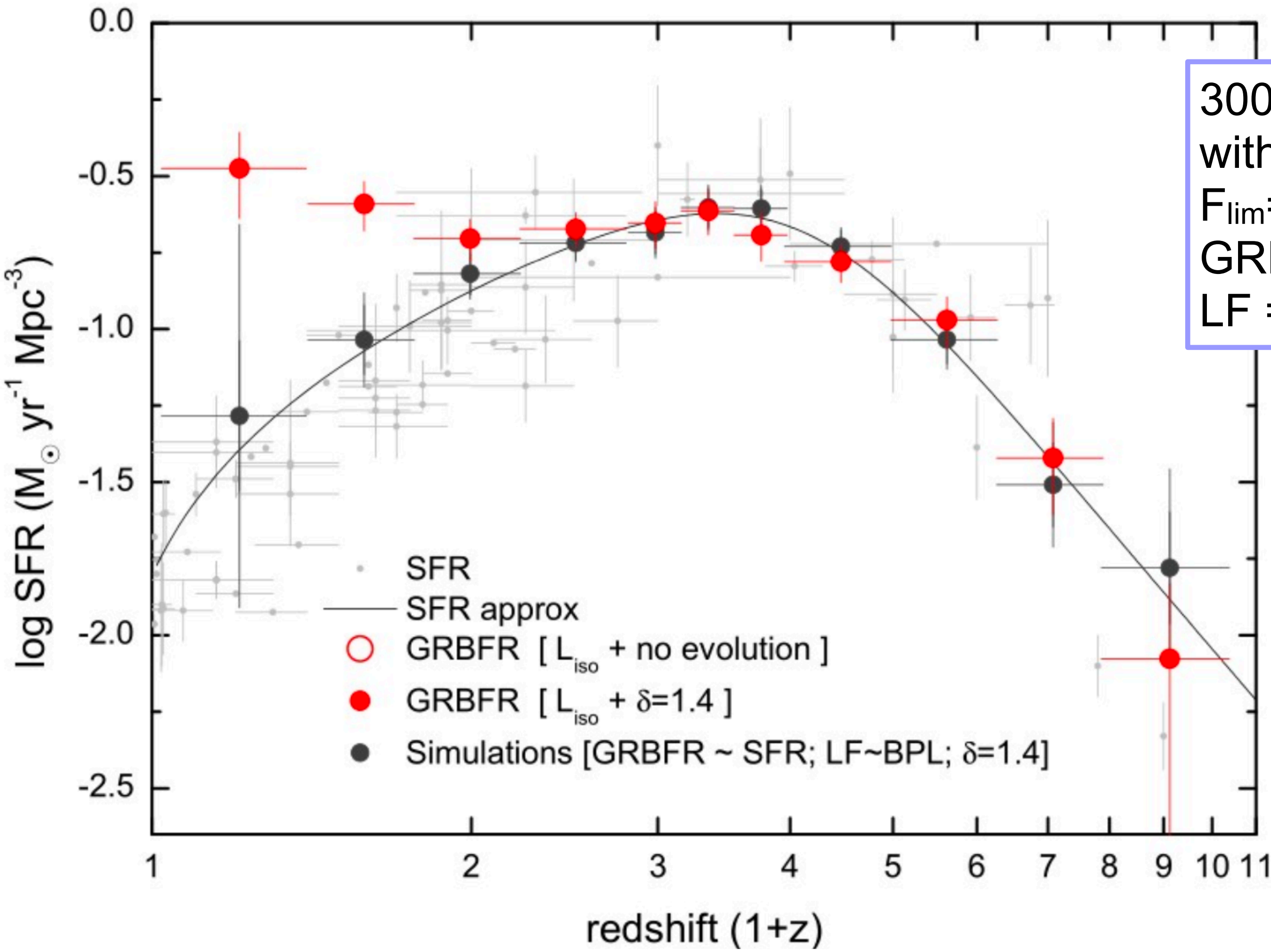

300 (z, L_{iso}) pairs
with $L_{iso} \geq 10^{47}$ erg s^{-1}
$F_{lim}=1.7\times10^{-7}$ erg cm^{-2} s^{-1}
GRBFR = SFR
LF = BPL

SFR: Hopkins (2004), Bouwens et al. (2011), Hanish et al. (2006), Thompson et al. (2006), Li (2008).

The present-time GRB luminosity and energy release functions

Cumulative luminosity function: $\ln \psi(L'_i) = \sum_{j=2}^{i} \ln\left(1 + \frac{1}{N'_j}\right)$

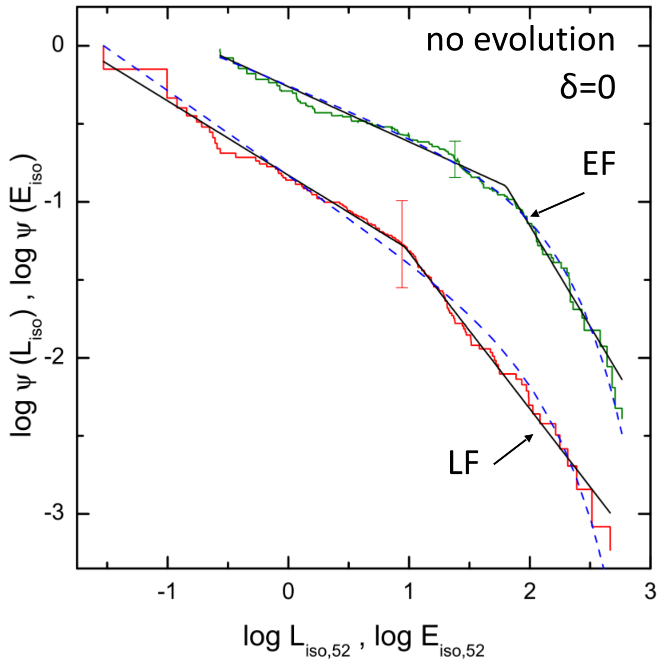

Best fit:
LF with BPL
(α_1~-0.3, α_2~-1);
EF with CPL
(α~-0.3,
E_{cut}~(2–4)×10^{54} erg).

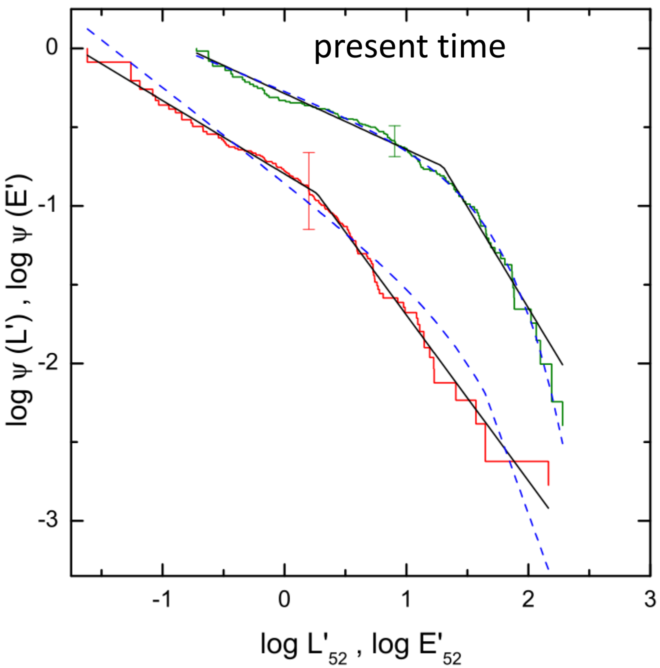

The existence of a sharp cutoff of the isotropic energy distribution of KW and *Fermi*/GBM GRBs around ~ 1−3×10^{54} erg was suggested recently by Atteia et al. (2017).

The present-time GRB luminosity and energy release functions: waiting mode

BPL:

$$\psi(x) \propto \begin{cases} x^{\alpha_1}, & x \le x_b \\ x_b^{(\alpha_1-\alpha_2)} x^{\alpha_2}, & x > x_b \end{cases}$$

α_1, α_2 – PL indices at the dim and bright distribution segments,

x_b – breakpoint of the distribution.

CPL:

$$\psi(x) \propto x^{\alpha} \exp(-x/x_{\mathrm{cut}})$$

α – PL index,

x_{cut} – cutoff luminosity (or energy).

LF and EF Fits with BPL and Cutoff PL

Data	Evolution (PL index)	Model	α_1	α_2	log $x_{b,52}$ (log $x_{\mathrm{cut},52}$)
$\psi(L')$	$\delta_L = 1.2$	BPL	$-0.28^{+0.04}_{-0.07}$	$-1.01^{+0.10}_{-0.28}$	$0.21^{+0.28}_{-0.18}$
$\psi(L')$	$\delta_L = 1.2$	CPL	$-0.45^{+0.08}_{-0.04}$	...	$1.67^{+0.19}_{-0.49}$
$\psi(E')$	$\delta_E = 1.1$	BPL	$-0.29^{+0.01}_{-0.09}$	$-1.01^{+0.02}_{-0.44}$	$0.80^{+0.44}_{-0.06}$
$\psi(E')$	$\delta_E = 1.1$	CPL	$-0.35^{+0.03}_{-0.04}$	...	$1.74^{+0.07}_{-0.11}$
$\psi(L_{\mathrm{iso}})$	no evolution	BPL	$-0.26^{+0.02}_{-0.05}$	$-0.99^{+0.05}_{-0.17}$	$0.78^{+0.17}_{-0.08}$
$\psi(L_{\mathrm{iso}})$	no evolution	CPL	$-0.38^{+0.04}_{-0.03}$	...	$2.02^{+0.11}_{-0.19}$
$\psi(E_{\mathrm{iso}})$	no evolution	BPL	$-0.26^{+0.01}_{-0.08}$	$-0.97^{+0.03}_{-0.44}$	$1.24^{+0.46}_{-0.08}$
$\psi(E_{\mathrm{iso}})$	no evolution	CPL	$-0.32^{+0.02}_{-0.04}$	...	$2.21^{+0.06}_{-0.09}$

Summary

- For the large sample of 317 long GRBs detected in a wide energy range, the luminosity and energy release functions and the GRB formation rate were computed using a non-parametric approach;
- The influence of instrumental selection:
  - in the triggered mode: the regions above the limits, corresponding to the bolometric fluence S_{lim} ~3×10^{-6} erg cm^{-2} (in the E_{iso} – z plane) and bolometric peak energy flux F_{lim} ~1×10^{-6} erg cm^{-2} s^{-1} (in the L_{iso} – z plane)may be considered free from the selection biases
  - In the waiting mode: S_{lim} ~1.6×10^{-6} erg cm^{-2} , F_{lim} ~1.7×10^{-7} erg cm^{-2} s^{-1};
- The GRB luminosity evolution (is present @ ~1.6σ), LF and EF, and the evolution of the GRBFR were estimated accounting for the instrumental bias;
- The derived luminosity evolution and isotropic-energy evolution indices $\delta L \sim 1.2$ and $\delta E \sim 1.1$ are more shallow than those reported in previous studies

Summary

- The shape of the derived LF is best described by a broken PL function with low- and high-luminosity slopes ~–0.3 and ~–1, respectively.
- The EF is better described by an exponentially cut off PL with the PL index ~–0.3 and a cutoff isotropic energy ~10^{54} erg.
- The derived GRBFR features an excess over the SFR at $z < 1$ and nearly traces the SFR at higher redshifts.

The talk is based on the papers Tsvetkova et al. (2017,2021)

Thank you!